Research in Astron. Astrophys. **2013** Vol. **13** No. **7**, 815–826
http://www.raa-journal.org *http://www.iop.org/journals/raa*

Research in Astronomy and Astrophysics

12 GHz methanol maser outflow from the massive star-forming region: G35.20–0.74 *

Qing-Zeng Yan[1], Bo Zhang[1,3], Zheng-Hong Tang[1] and Xing-Wu Zheng[2]

[1] Shanghai Astronomical Observatory, Chinese Academy of Sciences, Shanghai 200030, China; *qzyan@shao.ac.cn*
[2] School of Astronomy and Space Science, Nanjing University, Nanjing 210093, China
[3] Max-Plank-Institut für Radioastronomie, Auf dem Hügel 69, 53121 Bonn, Germany

Received 2012 September 29; accepted 2012 November 1

Abstract We report the internal proper motions of 12 GHz methanol masers in massive star-forming region G35.20–0.74 observed with the Very Long Baseline Array (VLBA) at four epochs spanning about 1.5 yr. Two groups of maser features were detected, groups A and B, and the latter that had a V-shaped spatial distribution is likely tracing the north outflow in G35.20–0.74. We present a three-dimensional model for the kinematics of these masers, by assuming the interstellar medium was blown by the stellar wind from the driving source (G35.2N) of the outflow. Adopting a position angle of $\sim 81^\circ$ for the main axis of the outflow from previous studies, we estimate an inclination of $35^\circ \pm 5.5^\circ$, a velocity of 8.1 ± 0.7 km s^{-1} for the stellar wind along the main axis and an expansion speed gradient of 0.05 ± 0.016 km s^{-1} AU^{-1}. From the model, we derive the age of the north outflow in G35.20–0.74 to be $\sim 1.6 \times 10^4$ yr.

Key words: masers — ISM: molecules — stars: kinematics — stars: individual (G35.20–0.74) — stars: winds, outflows

1 INTRODUCTION

G35.20–0.74 (IRAS 18556+0136) is a high-mass star-forming region at a distance of $2.19^{+0.24}_{-0.20}$ kpc (Zhang et al. 2009). The first detection of this molecular cloud was made by Brown et al. (1982) associated with the previously reported H_2O maser line (Batchelor et al. 1980). Previous observations indicate that G35.20–0.74 contains an early B-type star surrounded by an ultra compact H II region (Dent et al. 1984) with a bipolar jet driven outflow (Matthews et al. 1984; Dent et al. 1984, 1985a). G35.20–0.74 also shows a large rotating disk with a position angle $\sim 130^\circ$ east of north (Dent et al. 1985b; Little et al. 1985). OH and H_2O masers are located at the core of the flow, and appear to trace the inner edge of a molecular disk (Tapia et al. 1985; Brebner et al. 1987; Forster & Caswell 1989; Walther et al. 1990; Comoretto et al. 1990; Caswell et al. 1995; Hutawarakorn & Cohen 1999).

Heaton & Little (1988) conducted observations of the radio emissions at the center of the outflow with the Very Large Array (VLA) and revealed a structure with an optically thick central source that has collinear and optically thick lobes orientated north-south on either side. These findings support an argument that a bipolar molecular outflow is driven from the central source. They proposed

* Supported by the National Natural Science Foundation of China.

that the large difference in position angle between the CO and radio was due to precession of a collimated, ionized jet, and this interpretation was given further support by Little et al. (1998). A higher resolution VLA observation of this region by Gibb et al. (2003) shows that three concentrations of radio continuum emissions break up into 11 individual sources, all lying along the outflow. The central source is divided into two sources, a weaker southern component plus a stronger northern component associated with IRAS 18556+0136 (hereafter G35.2N), with a spectral index typical of a UC H II region, which is claimed to be the driving source of the radio jet. The $H^{13}CO^+$ peaks towards the location of a new millimeter source, G35MM2, which marks the position of a deeply embedded massive young stellar object and is the most likely candidate for driving much of the large-scale CO flow.

A high spatial resolution observation was made by Birks et al. (2006) using the Berkeley Illinois Maryland Association Array (BIMA). They observed ^{12}CO $J = 1 \rightarrow 0$, $C^{17}O$ $J = 1 \rightarrow 0$ and the 2.7 mm continuum. Their integrated ^{12}CO $J = 1 \rightarrow 0$ map shows another north CO outflow in addition to the northeast-southwest one, which means that the northeast-southwest CO outflow may not be the only one. They argued that the source G35MM2 is a more likely candidate for the source driving the northeast-southwest CO outflow than G35.2N. NH_3 emission was observed by Little et al. (1985); Codella et al. (2010). The CO outflow was also observed by López-Sepulcre et al. (2009), and their conclusion was consistent with the former observations.

An observation in the near-infrared at the K band of G35.20–0.74 by Walther et al. (1990) shows that a bipolar reflection nebula is oriented in the north-south direction. A source located $\sim 3''$ south of the radio source G35.2N was speculated to be causing emissions from the nebula. More recent near-infrared band observations by Fuller et al. (2001) have shown that the reflection nebula is still visible at the L' band, although its appearance supports the idea of a north-south jet emerging from G35.2N. They also claimed that the OH masers as seen by Hutawarakorn & Cohen (1999) trace a circumstellar disk because they lie near the base of the jet and are linearly distributed at a position angle perpendicular to the jet. De Buizer et al. (2005); De Buizer (2006) observed G35.20–0.74 at mid-infrared wavelengths. These observations revealed an extended source that has the shape of a comet with the masers concentrated around the head. They concluded that the source is dominated at wavelengths greater than 3 μm by re-radiated thermal emission from the outflow cavity rather than by scattered light. The near- and mid-infrared emission appears to indeed be tracing the outflow from the UC H II region and most of the masers are involved in this outflow. However, the nature of those maser's relationship with the radio continuum emission is still unclear.

The 6.7 GHz methanol maser in G35.20–0.74 was observed by both Sugiyama et al. (2008); Surcis et al. (2012) using the Japanese very-long-baseline interferometry (VLBI) network (JVN) and the European VLBI network (EVN), respectively. The methanol features obtained by them are divided into two groups with a distance of 5000 AU. Surcis et al. (2012) concluded that only one of the two groups is associated with the outflow, and they also observed the polarization of the magnetic field traced by the masers.

In this paper, we present internal proper motion measurements of 12 GHz CH_3OH masers toward G35.20–0.74 using the Very Long Baseline Array (VLBA). Internal proper motions of maser features can clarify the relationship between masers and outflow. Moreover, internal proper motions can help determine some physical parameters of the outflow. If the methanol maser in G35.20–0.74 really is a tracer of the outflow, the internal proper motions of the maser features would be close to the direction of the CO outflow. Combined with the accurately determined distance to this region, we can propose a three-dimensional kinetic model for the outflow in G35.20–0.74.

2 OBSERVATIONS AND DATA REDUCTION

Our observations of 12 GHz methanol masers in G35.20–0.74 were conducted under the VLBA program BR100E on 2005 October 30, 2006 April 7 and October 7, and 2007 April 16. This sampling

provides nearly maximum sensitivity for parallax detection and ensures that we can separate the absolute proper motion from the sinusoidal parallax effect (Reid et al. 2009). We used four adjacent frequency bands with 4 MHz bandwidth in dual circular polarization. The second band contained the maser signals and was centered at a local standard of rest velocity ($V_{\rm LSR}$) of 31 km s^{-1}. We observed two ICRF sources: J1800+3848 and J1800+7828 (Ma et al. 1998), at the beginning, middle and end of the observations, which were used for phase-referencing in order to monitor delay and electronic phase differences among the observing bands. The correlation was set up with the VLBA correlator in Socorro, New Mexico. The correlation outputs consisted of 256 channels, yielding a frequency spacing of 15.4 kHz, corresponding to a velocity resolution of 0.38 km s^{-1}.

We calibrated the correlated data using the National Radio Astronomy Observatory's Astronomical Image Processing System (AIPS). We used the system temperature and the antenna gain information provided in the VLBA calibration tables for the amplitude calibration, and adjusted the amplitude of the interferometer visibility for the small effects of biases in the threshold levels of the data samplers at each station. The phase of the observed visibility of G35.20–0.74 was corrected by taking the following steps. Firstly, the instrumental single-band delay and the phase difference among all eight 4 MHz bands were derived by a "manual phase-calibration," which was done by selecting a single scan of the strong continuum calibrator, fitting fringe patterns to the data for each frequency band, and then shifting delays and phases to G35.20–0.74 to remove the effects. Secondly, we shifted the frequency axes of the maser interferometer spectra to compensate for the Doppler shift caused by time-variant projection of the Earth's orbit and spin toward the source, to keep a constant $V_{\rm LSR}$ in any given spectral channel. Finally, we used a single spectral channel with a strong and compact maser source at $V_{\rm LSR}$ of 28.31 km s^{-1} (see Fig. 1) to provide a "maser phase reference." The visibilities of the phase reference channel were fringe fitted to derive the residual fringe phases and rates introduced by differences in atmospheric fluctuations at each station and by errors in the nominal source coordinates adopted in the correlation. The fringe amplitude, rate and phase correction derived from the reference phase channel were applied to all channels of the maser data.

Once all the maser data were calibrated, we made images of the masers emissions in spectral channels, using the AIPS task IMAGR with uniform weighting. We noticed that the cross-power spectra of long baselines which contain antennas in Brewster, Washington, Mauna Kea, Hawaii and St. Croix, U.S. Virgin Islands were rather noisy compared to other baselines. This is probably because the maser sources were resolved by the long baselines. Thus, we excluded these antennas in mapping the maser emission. A total of five channels with relatively strong maser emission were mapped. Their corresponding $V_{\rm LSR}$ values are 29.4, 28.7, 28.3, 27.9 and 27.5 km s^{-1} respectively. In order to provide precise determination of the maser spot parameter, we fitted an elliptical Gaussian brightness distribution to the maser spots at all four epochs, using the AIPS task JMFIT.

3 SPATIAL DISTRIBUTION OF MASERS AND INTERNAL PROPER MOTIONS

Figure 1 shows the cross-power spectra of emission from the 12 GHz methanol maser obtained by the VLBA baseline from KP to FD at all four epochs. The CH_3OH emission is spread over values for $V_{\rm LSR}$ ranging from about 27.5 to 29.4 km s^{-1}. The spectrum appears rather stable from epoch to epoch during about 1.5 yr. The peak of the spectrum is at a $V_{\rm LSR}$ value of 28.31 km s^{-1}, which is different from 31 km s^{-1} at 12 GHz but consistent with 6.7 GHz in a previous single dish observation by Caswell et al. (1995) using the Parkes telescope.

Similar to the 6.7 GHz methanol maser observed by Sugiyama et al. (2008); Surcis et al. (2012), the 12 GHz maser features can also be divided into two groups with different positions, A and B, which are consistent with those of 6.7 GHz observations. The $V_{\rm LSR}$ of masers in group A range from 27.9 to 29.4 km s^{-1}, and those of group B range from 27.5 to 28.7 km s^{-1}.

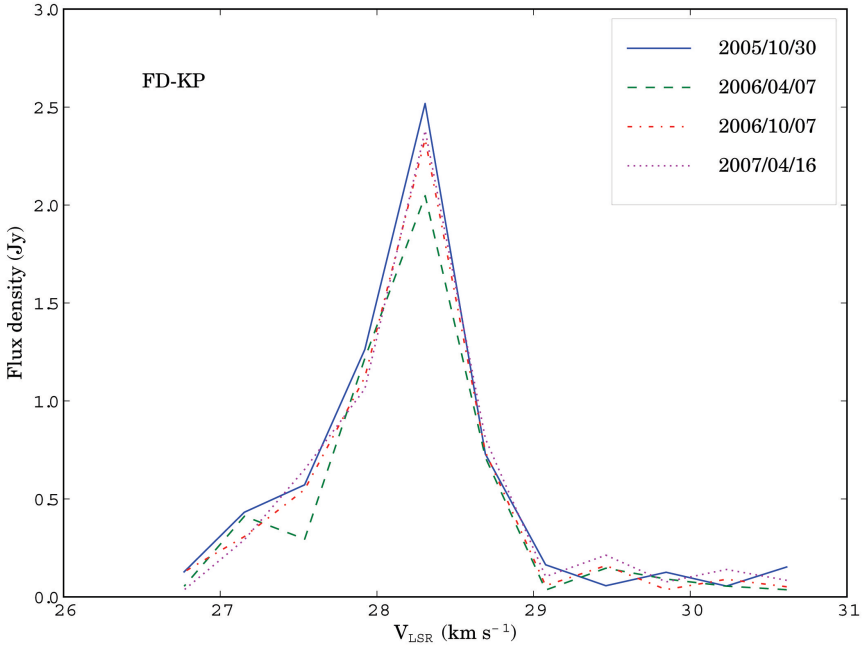

Fig. 1 Interferometer (scalar averaged cross-power amplitude over the full duration of the observation) spectra of the 12 GHz methanol maser towards G35.20–0.74 obtained with the VLBA baseline from FD to KP at four epochs. Observation dates are labeled in the top right corner of the panel. The $V_{\rm LSR}$ range from 26 to 31 km s^{-1}.

We consider the maser features at different epochs as being the same if their $V_{\rm LSR}$ are equal to each other within 0.38 km s^{-1}, and if their positions are within 3 mas, which corresponds to 20.8 km s^{-1} within 1.5 yr. In other words, if two maser spots are in adjacent channels and in the same beam, they can be considered to be the same. Based on these criteria, we identified five maser features in each group.

The position offsets of maser features relative to the reference maser feature are obtained by using the AIPS task JMFIT. The proper motions relative to the reference maser feature are calculated by performing a weighted linear least-squares fit to the position offsets against the observation time. Since those proper motions are all relative to the reference maser feature, the common part should be caused by the reference maser feature. We estimate a systematic proper motion of (–0.01±0.15, –0.53±0.42) mas yr^{-1} with the other nine maser features using the least- squares method. The large inaccuracy in the systematic proper motion is due to insufficient epochs of observation and a large difference between the proper motions of group A and those of group B. The internal proper motion of each maser feature is obtained by subtracting the systematic proper motion from the original relative proper motion. Therefore, errors arising from inaccuracies in internal proper motion are mostly due to large errors in the systematic proper motion.

Table 1 lists parameters of all the identified 12 GHz CH_3OH maser features in G35.20–0.74.

Figure 2 shows the spatial distribution and internal proper motions of all the 12 GHz maser features. For comparison, we also plot the spatial distribution of the 6.7 GHz CH_3OH maser features measured by Surcis et al. (2012). We adopted an absolute position $\alpha_{\rm J2000}$=18$^{\rm h}$58$^{\rm m}$13.053$^{\rm s}$ and $\delta_{\rm J2000}$=01°40′35.68″by Xu et al. (2009) for the 6.7 GHz reference maser feature. For the absolute position of the 12 GHz reference maser feature, we adopted $\alpha_{\rm J2000}$= 18$^{\rm h}$58$^{\rm m}$13.0517$^{\rm s}$ and $\delta_{\rm J2000}$=

Table 1 Parameters and Internal Proper Motions of Maser Features

Group	$V_{\rm LSR}$ (km s^{-1})	Flux (mJy)	E-W offset (mas)	N-S offset (mas)	E-W proper motion (mas yr^{-1})	N-S proper motion (mas yr^{-1})
B	28.7	159.9	-8.80 ± 0.05	18.31 ± 0.11	-0.01 ± 0.19	0.03 ± 0.59
B	28.7	365.7	6.35 ± 0.04	-1.17 ± 0.10	0.08 ± 0.16	-0.01 ± 0.62
A	28.7	100.1	-1558.47 ± 3.04	1764.79 ± 3.10	-0.64 ± 0.15	0.21 ± 0.62
A	28.7	124.4	-1559.06 ± 3.02	1761.41 ± 3.07	-0.20 ± 0.17	-0.24 ± 1.01
B	28.3	1358.4	0.001 ± 0.01	-0.00 ± 0.02	0.01 ± 0.15	0.53 ± 0.42
A	28.3	138.9	-1552.66 ± 3.04	1823.68 ± 3.09	-0.11 ± 0.15	-0.16 ± 0.42
B	27.9	100.0	-11.41 ± 3.03	32.03 ± 3.07	0.25 ± 0.15	-0.37 ± 0.51
B	27.5	329.4	0.80 ± 0.02	-6.66 ± 0.06	0.14 ± 0.16	0.01 ± 0.58
A	29.4	219.7	-1542.22 ± 3.01	1863.88 ± 3.04	-0.09 ± 0.15	0.31 ± 0.43
A	29.4	259.5	-1543.45 ± 3.01	1859.20 ± 3.04	-0.08 ± 0.15	0.02 ± 0.43

Notes: Col. (1) is the group in which the 12 GHz methanol maser features are located. Cols. (2) and (3) are $V_{\rm LSR}$ and fluxes of the maser features, respectively. Cols. (4) and (5) are unweighted averages of offsets obtained by the AIPS task JMFIT at four epochs. Cols. (6) and (7) are the results of fitting internal proper motions of maser features.

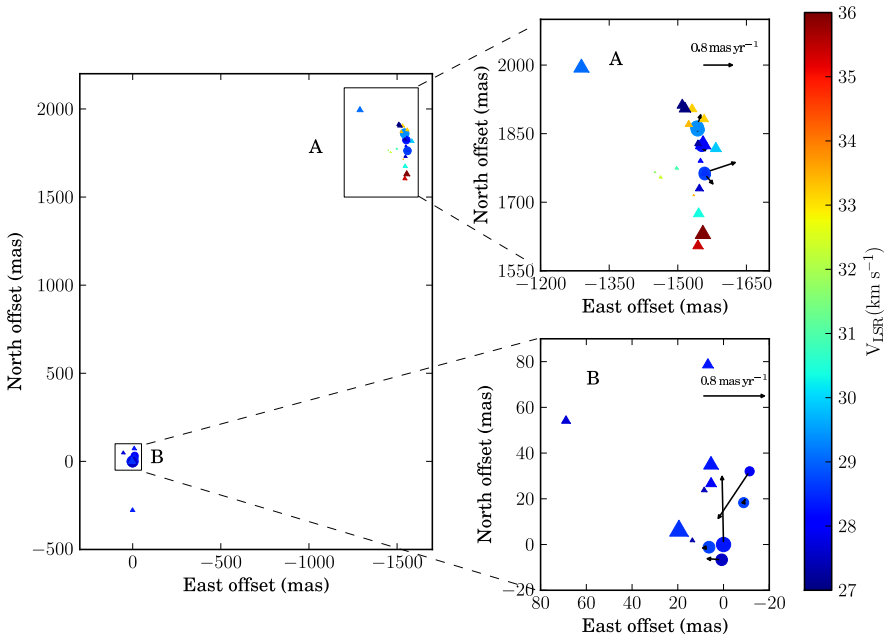

Fig. 2 Spatial distribution and internal proper motions of methanol maser features in G35.20–0.74. The colors denote the $V_{\rm LSR}$ ranging from 27.0 to 36.0 km s^{-1}. The methanol masers are divided into two groups, A and B. The circles and triangles mark the positions of maser features at 12 GHz (this paper) and 6.7 GHz (Surcis et al. 2012), respectively. The two species of methanol masers are aligned by assuming the reference maser feature at 6.7 GHz is at an absolute position reported by Xu et al. (2009). The coordinate origin is the position where the 12 GHz methanol reference maser feature is located, which is estimated to be $\alpha_{\rm J2000}$=18$^{\rm h}$58$^{\rm m}$13.0517$^{\rm s}$ and $\delta_{\rm J2000}$=01°40′35.674″ as reported by Zhang et al. (2009). The internal proper motions indicated with arrows are obtained by subtracting an averaged value of (μ_x, μ_y) = (–0.01, –0.53) mas yr^{-1} from the original proper motion of each maser feature relative to the reference feature.

$01^\circ40'35.674''$ from Zhang et al. (2009). Therefore, we align the maps of the 6.7 GHz and 12 GHz maser features by shifting the 6.7 GHz maser features 19.5 mas eastward and 6 mas northward.

Figures 3 and 4 show the contour maps of maser features at four epochs for groups A and B, respectively. Compared to group A, the maps of maser features in group B have much higher intensity. For group A, the images of the second epoch, 2006 April 7, are not as good as those of the other three epochs, because the antenna in Pie Town, New Mexico, was not available at the second epoch. As a consequence, the second epoch was not used in the fit of proper motion fitting for group A.

4 DISCUSSION

4.1 Outflow Traced by 12 GHz Methanol Masers

As mentioned by Surcis et al. (2012), the distance between the two groups is about 5000 AU. The consistent velocities of the two groups mean that they are probably embedded in the same region of the interstellar medium. However, we cannot draw any further relationship between the two groups according the existing observations. Although the two groups show a line structure, Surcis et al. (2012) considered that group B was associated with the outflow rather than the line structure based on their consistent velocities. At 12 GHz, the intensity of most of the maser features in group B is higher than those in group A. We consider group A to be a tracer of an accretion disk or something else, but not related to group B which is most likely tracing the north outflow. Therefore, our discussion is mainly focused on group B.

The NH_3 and CO observations show a northeast-southwest CO outflow with a rotating interstellar disk in G35.20–0.74. However, the north-south distributed radio continuum emission obtained by Gibb et al. (2003) does not coincide with the direction of northeast-southwest CO outflow. The CO emissions obtained by Birks et al. (2006) also show another CO outflow towards the north in addition to the northeast-southwest CO outflow. Therefore, Gibb et al. (2003) and Birks et al. (2006) both conclude that there is more than one outflow in G35.20–0.74. However, the driving sources of the two outflows are still unclear. Birks et al. (2006) considered the source G35MM2 to be a more likely candidate for the source driving the northeast-southwest CO outflow than G35.2N (see Fig. 5).

The relationship between methanol masers and mid-infrared emissions of G35.20–0.74 was discussed by De Buizer (2006). The group B methanol masers are almost at the head of the comet-shaped cloud as shown in Figure 5. The internal proper motion of the feature representing the 12 GHz methanol reference maser is pointing directly towards the end of the comet. This is more convincing evidence suggesting the existence of the north outflow in G35.20–0.74. The north CO outflow shown in Figure 5 is also consistent with mid-infrared emissions.

According to the internal proper motions, we fitted the position of the central star. Each maser feature corresponds to an angle between its internal proper motion and position vector relative to the central star. The position should minimize the sum of squares for those angles, and it should be near the southernmost maser feature considering the thickness of the accretion disk. The calculated result is about $(0.01, -6.51)$ mas. We believe that this position, which is marked by a red star in Figure 5, is where the driving source of the north outflow is located. G35.2N, with an absolute position of $\alpha_{\rm J2000}$= $18^{\rm h}58^{\rm m}13.02^{\rm s}$ and $\delta_{\rm J2000}$= $01^\circ40'36.20''$ (Gibb et al. 2003), is very close to the central star. Therefore, it may be the radio counterpart of the central star considering the relative astrometric uncertainty. Further observation is needed to confirm the absolute position of G35.2N.

The methanol masers in G35.20–0.74 show a V-shaped distribution. The scale of the V-shape shown by methanol masers, however, is much smaller than that shown by OH and H_2O masers as mentioned by De Buizer (2006). This V-shape may draw the outline of a cavity excavated by the outflow. With those internal proper motions and the distribution of methanol masers, we propose a three-dimensional kinematic model for the interstellar medium traced by maser features and blown by the stellar wind driven by the central star.

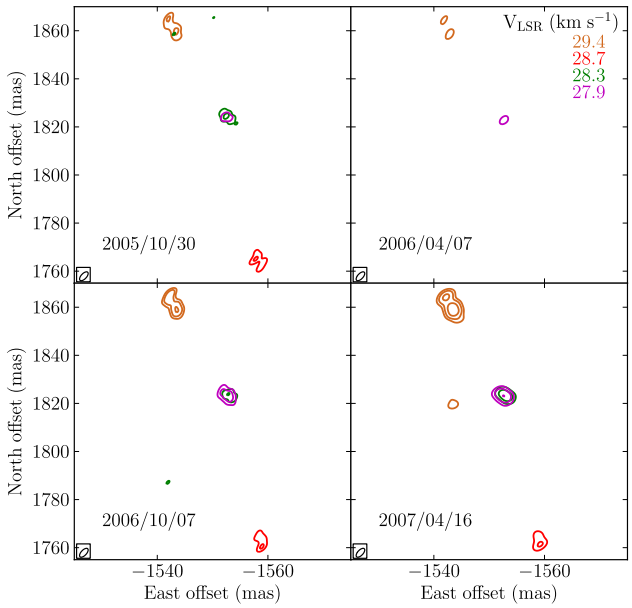

Fig. 3 Maps of maser features in four channels (at different $V_{\rm LSR}$) for each epoch of group A. The observation date is labeled in the bottom left corner of each panel. The colors denote different $V_{\rm LSR}$ ranging from 29.4 to 27.9 km s^{-1}. The restoring beam is indicated in the bottom left corner of each panel with a size of 3.8 mas×1.2 mas at a position angle (East to North) of 106°. The position offset of each maser feature is relative to the reference maser feature located at an absolute position of $\alpha_{\rm J2000}$= 18$^{\rm h}$58$^{\rm m}$13.0517$^{\rm s}$ and $\delta_{\rm J2000}$= 01°40′35.674″.

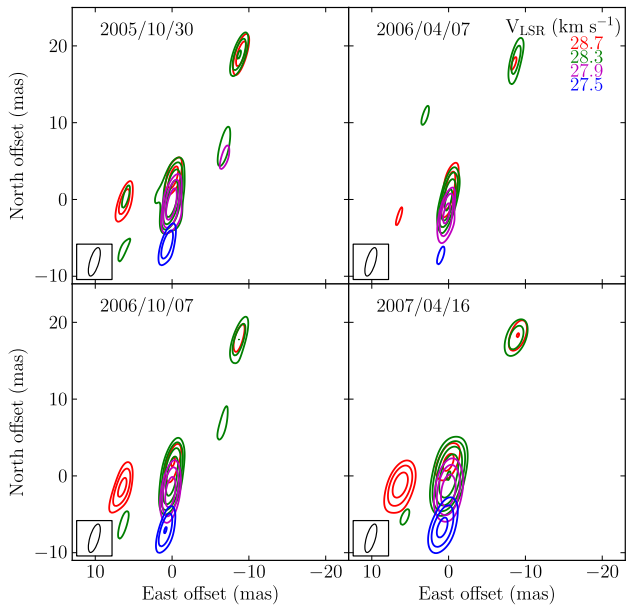

Fig. 4 The same as Fig. 3 but for group B.

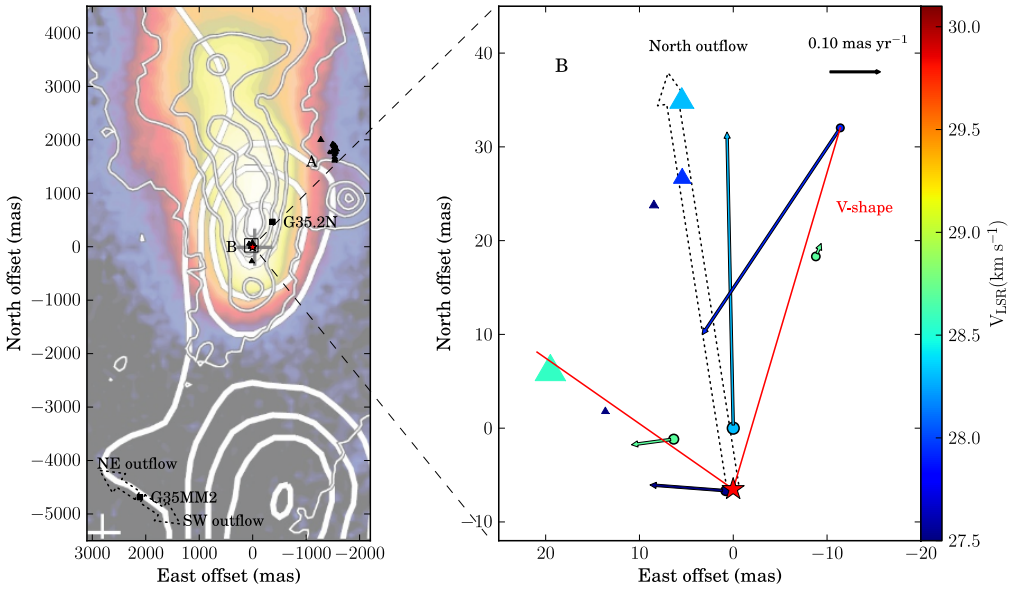

Fig. 5 Internal proper motions of maser spots in Group B. The background of the left panel is the mid-infrared emission observed by De Buizer (2006). The heavy white contours denote the 15 GHz radio continuum emissions observed by Heaton & Little (1988), and the light white contours denote the L' band mid-infrared emission observed by Fuller et al. (2001). The radio continuum sources G35MM2 and G35.2N are marked with rectangles in the left panel. The solid colored arrows in the right panel denote the internal proper motions of 12 GHz methanol maser features. The circles and triangles mark the positions of methanol masers at 12 GHz (this paper) and 6.7 GHz (Surcis et al. 2012), respectively. The dashed arrows denote CO outflows observed by Birks et al. (2006). The red line denotes the V-shaped distribution of methanol maser features, and the central star is marked with a red star.

4.2 Outflow Model

The bipolar outflows from young protostars have been studied in great detail over the last few decades (Bachiller 1996; Bachiller & Tafalla 1999; Su et al. 2004; Seifried et al. 2012; Wu et al. 2004). However, the driving mechanisms of bipolar outflows remain in doubt. The theoretical investigation of bipolar outflows is still struggling to progress. Be that as it may, some consensus has been reached. For example, the bipolar outflows are magnetically driven (Seifried et al. 2012), and they are an inevitable phenomenon in the process of star formation. As mentioned by Bachiller & Tafalla (1999), there are two main categories of molecular outflow models: wide angle wind models and jet models. Since the spatial distribution of the masers is not that collimated, in this case we prefer the wide angle wind models.

Here, we present an expanding kinematic outflow model to explain the north outflow traced by the 12 GHz methanol masers of G35.20–0.74. We assume that the stellar wind is driven by the central star, and the movement of the interstellar medium traced by the maser features and blown by stellar wind should be concentric expansion. Combining the internal proper motions and radial velocities ($V_{\rm LSR}$), we calculated the three-dimensional velocity vectors for all maser features. However, we measured only the two-dimensional positions (east and north offsets) of the maser features. Therefore, we should estimate the radial offsets of the maser features. First, we set the origin of the coordinate system to the position of the central star. Then, we adjusted the radial offsets of

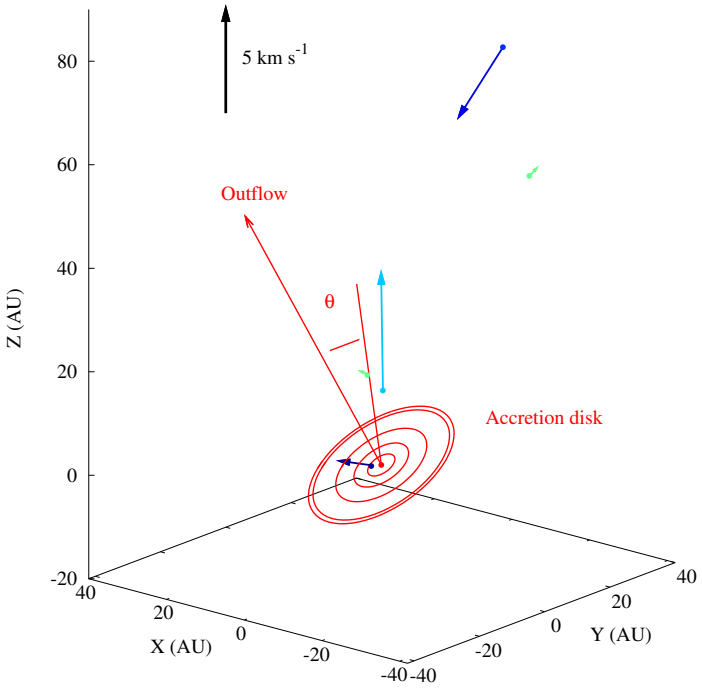

Fig. 6 Three-dimensional outflow model for G35.20–0.74. The X, Y and Z axes denote RA, radial and Dec offsets from the maser features, respectively. The dots denote the maser features with colors representing the $V_{\rm LSR}$ except for the red one which marks the central star. The red arrow represents the direction of the main axis for stellar wind. The colored arrows denote the internal proper motions of 12 GHz methanol maser features. The red circles denote the position of the accretion disk. Angle θ is the included angle between each maser feature's position vector and the main axis.

maser features by minimizing the angle between the internal proper motion and the position vector for each maser feature. Due to the small difference among the $V_{\rm LSR}$ of the maser features, the radial offsets should be no greater than 20 AU during the lifecycle of methanol masers. Three-dimensional velocities and positions of 12 GHz methanol maser features are shown in Figure 6.

The direction of the main axis of the outflow is denoted by spherical polar coordinates (1, β, α), corresponding to $(\cos\alpha\cos\beta, -\sin\alpha, \cos\alpha\sin\beta)$ in Cartesian coordinates. The position angle β (east to north) is adopted as 81° according to CO (Birks et al. 2006) and 2.2 μm (Walther et al. 1990) observations. The inclination α is a parameter to be estimated. For each maser feature, there is an angle θ between the main axis and the position vector as shown in Figure 6. The maser expansion speed decreases with increasing θ (from the main axis to the accretion disk) in proportion to its cosine (Shu et al. 1991). In addition, we add a gradient in expansion speed that is proportional to distance from the central star.

$$\boldsymbol{V}(\theta, \boldsymbol{r}) = (V_{\rm max}\cos\theta - Kr)\frac{\boldsymbol{r}}{r}, \tag{1}$$

$$\cos\theta = \frac{x\cos\alpha\cos\beta - y\sin\alpha + z\cos\alpha\sin\beta}{r}, \tag{2}$$

where r is the distance from the central star to maser features, $\boldsymbol{V}(\theta, \boldsymbol{r})$ is the velocities of the maser features at direction θ and distance r, $V_{\rm max}$ is the stellar wind velocity along the main axis, K is the

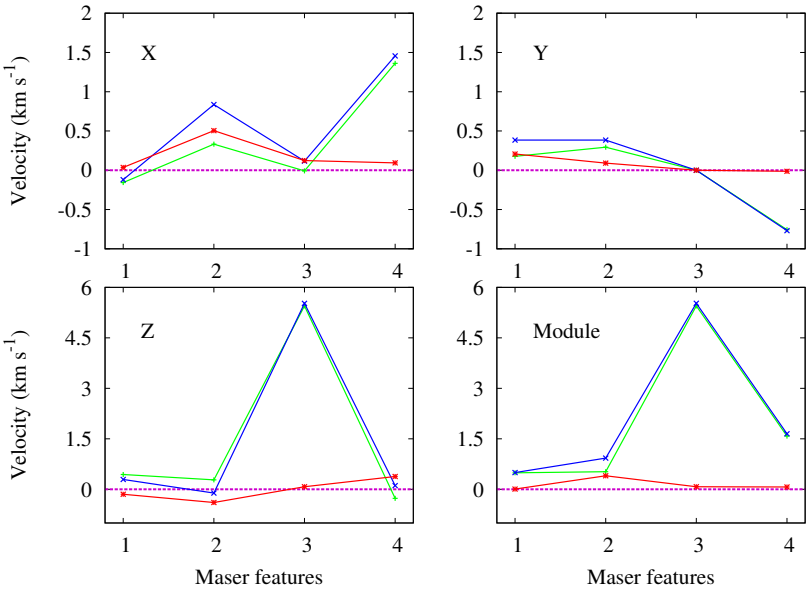

Fig. 7 Fitting result of the outflow model. The *green, blue, red* and *purple* lines denote model fitted values, observed values, post-fit residuals, and zero lines, respectively.

expansion speed gradient with the distance r, and (x, y, z) are components of the position vectors of maser features relative to the central star. α, $V_{\rm max}$ and K are unknown parameters to be estimated.

The blue maser feature at (–25, 7.6, 84) AU shown in Figure 6, with a large internal proper motion that is opposite compared to other features and which lies far from the central star, is believed to show an infall movement, and is most likely beyond the stellar wind. Therefore, it was excluded when doing model fitting. The number of parameters is three, and we derived 12 equations according to the vector equations. Therefore, we can estimate the parameters using the least-squares method. The estimated values of α, $V_{\rm max}$ and K are $35^\circ \pm 5.5^\circ$, 8.1 ± 0.8 km s^{-1} and 0.05 ± 0.016 km s^{-1} AU^{-1} respectively. The fitting result is shown in Figure 7. The root mean square of residuals after the fit is 0.28 km s^{-1}, and the observed values are significant compared these residuals.

4.3 Physical Parameters of Outflow

According to the fitting result, we can estimate some parameters of the north outflow. The inclination of the main outflow axis is about 35°. The methanol maser and mid-infrared observations both point to a conclusion that only the northern half of the north-south outflow was detected. However, the radio continuum emission (Gibb et al. 2003) and 2.2 μm observation (Walther et al. 1990) show the entire north-south outflow. For the CO emission observed by Birks et al. (2006), part of the red shell may also belong to the north-south outflow. This may be due to the nonuniform distribution of the materials surrounding the central star.

The maximum velocity of the interstellar medium near the central star is about 8.1 km s^{-1}, corresponding to 0.64 mas yr^{-1} (6.6 km s^{-1}) projected on a celestial sphere at a distance of 2.19 kpc. The mean velocity of the north CO outflow is about 7.43 km s^{-1} (Birks et al. 2006), and this is consistent with our modeled value of 6.6 km s^{-1}. We believe that the stellar wind has nearly the same

velocity, but stays constant along the main axis. According to the radio continuum and mid-infrared emissions of G35.20–0.74, the scale of the north outflow is estimated to be about $10''$. Therefore, the age of the north molecular outflow is calculated to be $\sim 1.6 \times 10^4$ yr. The average age of the high mass outflows is about 9.8×10^4 yr (Wu et al. 2004), and the kinematical timescale obtained by CO spectroscopy ranges from about 10^3 yr to about 10^5 yr (Bachiller & Tafalla 1999). Our result is consistent with both of them, and the north outflow of G35.20–0.74 is quite young.

5 CONCLUSIONS

The four epoch observations of methanol masers in G35.20–0.74 with the VLBA helped us to measure the internal proper motions of maser features in it. From the study, we draw the following main conclusions about molecular outflows from these young stars and protostars.

(1) The direction of internal proper motion of the reference maser feature is in good agreement with the continuum and mid-infrared emissions of G35.20–0.74. The 12 GHz methanol maser features trace the north CO outflow in G35.20–0.74. The V-shaped spatial distribution of the 12 GHz and 6.7 GHz CH_3OH maser features indicates that methanol masers in G35.20–0.74 are most likely located at the edge of the cavity excavated by the north outflow.
(2) At least two outflows were confirmed in G35.20–0.74. The methanol masers and mid-infrared emissions in G35.20–0.74 both trace the northern half of the north-south outflow but the other half may be not excited due to a nonuniform distribution of the interstellar medium surrounding the central star.
(3) We performed a three-dimensional wide angle model fitting for the north outflow. The inclination angle of the outflow's main axis is about 35°. G35.2N may be the driving source of the north outflow considering the relative astrometric uncertainty. The velocity of the stellar wind along the main axis near the central star is about 8.1 km s^{-1}, corresponding to 0.64 mas yr^{-1} projected on the celestial sphere at a distance of 2.19 kpc. The age of the north outflow is estimated to be $\sim 1.6 \times 10^4$ yr, which is quite young.
(4) Massive star-forming region G35.20–0.74 has one of the most collimated bipolar outflows (northeast-southwest outflow driven by G35MM2) located within the structure, and it is a good case for studying the relationship of masers and bipolar outflows. Due to insufficient observations, the inaccuracies of the fitting result for internal proper motion are a little large. Further observations are needed to improve our result.

Acknowledgements This work was supported by the National Science Foundation of China (Grant Nos. 11073046 and 11133008).

References

Bachiller, R. 1996, ARA&A, 34, 111
Bachiller, R., & Tafalla, M. 1999, in NATO ASIC Proc. 540: The Origin of Stars and Planetary Systems, eds. C. J. Lada, & N. D. Kylafis, 227
Batchelor, R. A., Caswell, J. L., Haynes, R. F., et al. 1980, Australian Journal of Physics, 33, 139
Birks, J. R., Fuller, G. A., & Gibb, A. G. 2006, A&A, 458, 181
Brebner, G. C., Heaton, B., Cohen, R. J., & Davies, S. R. 1987, MNRAS, 229, 679
Brown, A. T., Little, L. T., MacDonald, G. H., & Matheson, D. N. 1982, MNRAS, 201, 121
Caswell, J. L., Vaile, R. A., Ellingsen, S. P., Whiteoak, J. B., & Norris, R. P. 1995, MNRAS, 272, 96
Codella, C., Cesaroni, R., López-Sepulcre, A., et al. 2010, A&A, 510, A86
Comoretto, G., Palagi, F., Cesaroni, R., et al. 1990, A&AS, 84, 179
De Buizer, J. M., Radomski, J. T., Telesco, C. M., & Piña, R. K. 2005, ApJS, 156, 179

De Buizer, J. M. 2006, ApJ, 642, L57
Dent, W. R. F., Little, L. T., & White, G. J. 1984, MNRAS, 210, 173
Dent, W. R. F., Little, L. T., Kaifu, N., Ohishi, M., & Suzuki, S. 1985a, A&A, 146, 375
Dent, W. R. F., Little, L. T., Sato, S., Ohishi, M., & Yamashita, T. 1985b, MNRAS, 217, 217
Forster, J. R., & Caswell, J. L. 1989, A&A, 213, 339
Fuller, G. A., Zijlstra, A. A., & Williams, S. J. 2001, ApJ, 555, L125
Gibb, A. G., Hoare, M. G., Little, L. T., & Wright, M. C. H. 2003, MNRAS, 339, 1011
Heaton, B. D., & Little, L. T. 1988, A&A, 195, 193
Hutawarakorn, B., & Cohen, R. J. 1999, MNRAS, 303, 845
Little, L. T., Dent, W. R. F., Heaton, B., Davies, S. R., & White, G. J. 1985, MNRAS, 217, 227
Little, L. T., Kelly, M. L., & Murphy, B. T. 1998, MNRAS, 294, 105
López-Sepulcre, A., Codella, C., Cesaroni, R., Marcelino, N., & Walmsley, C. M. 2009, A&A, 499, 811
Ma, C., Arias, E. F., Eubanks, T. M., et al. 1998, AJ, 116, 516
Matthews, N., Little, L. T., MacDonald, G. H., & Nyman, L.-A. 1984, A&A, 136, 282
Reid, M. J., Menten, K. M., Brunthaler, A., et al. 2009, ApJ, 693, 397
Seifried, D., Pudritz, R. E., Banerjee, R., Duffin, D., & Klessen, R. S. 2012, MNRAS, 422, 347
Shu, F. H., Ruden, S. P., Lada, C. J., & Lizano, S. 1991, ApJ, 370, L31
Su, Y.-N., Zhang, Q., & Lim, J. 2004, ApJ, 604, 258
Sugiyama, K., Fujisawa, K., Doi, A., et al. 2008, PASJ, 60, 23
Surcis, G., Vlemmings, W. H. T., van Langevelde, H. J., & Hutawarakorn Kramer, B. 2012, A&A, 541, A47
Tapia, M., Roth, M., Persi, P., & Ferrari-Toniolo, M. 1985, MNRAS, 213, 833
Walther, D. M., Aspin, C., & McLean, I. S. 1990, ApJ, 356, 544
Wu, Y., Wei, Y., Zhao, M., et al. 2004, A&A, 426, 503
Xu, Y., Voronkov, M. A., Pandian, J. D., et al. 2009, A&A, 507, 1117
Zhang, B., Zheng, X. W., Reid, M. J., et al. 2009, ApJ, 693, 419